

Modeling the Mechanosensitivity of Fast-Crawling Cells on Cyclically Stretched Substrates

John J. Molina^{1,*} and Ryoichi Yamamoto^{1,2}

¹*Department of Chemical Engineering, Kyoto University, Kyoto 615-8510*

²*Institute of Industrial Science, The University of Tokyo, Tokyo 153-8505*

(Dated: August 29, 2018)

The mechanosensitivity of cells, which determines how they are able to respond to mechanical signals received from their environment, is crucial for the functioning of all biological systems. In experiments, cells placed on cyclically stretched substrates have been shown to reorient in a direction that depends not only on the type of cell, but also on the mechanical properties of the substrate, and the amplitude and rate of stretching. However, the underlying biochemical and mechanical mechanisms responsible for this realignment are still not completely understood. In this study, we introduce a computational model for fast crawling on cyclically stretched substrates that accounts for the sub-cellular processes responsible for the cell shape and motility, as well as the coupling to the substrate through the focal adhesion sites. In particular, we focus on the role of the focal adhesion dynamics, and show that the reorientation under cyclic stretching is strongly dependent on the frequency, as has been observed experimentally. Furthermore, we show that an asymmetry during the loading and unloading phases of the stretching, whether coming from the response of the cell itself, or from the stretching protocol, can be used to selectively align the cells in either the parallel or perpendicular directions.

arXiv:1807.02295v2 [physics.bio-ph] 28 Aug 2018

* john@cheme.kyoto-u.ac.jp

I. INTRODUCTION

The structure and function of cells is carefully regulated by the signals they receive from their environment. Of particular interest is the transfer of mechanical forces and stresses, which in turn are known to trigger specific biochemical responses inside the cell that can significantly alter their behavior, inducing changes in shape, size, motility, reorganization of the cytoskeleton, and even cell proliferation and differentiation[1, 2]. This last example is probably the most striking, given the bio-medical applications it promises. Carefully engineered bio-materials should allow us to control stem cell fate decisions, i.e., whether or not they divide or differentiate, and which specific cell lineage is chosen[3]. However, before this is possible, we need to have a fundamental understanding of the interactions between the cells and the chosen bio-material.

One of the preferred methods to probe the mechanical interaction of cells with their environment is to place them on an elastic substrate that is being periodically stretched along a given direction. Studying how the cells respond to this perturbation provides crucial information on its mechanosensing abilities. Following Iwadate et al.[4–7], it is useful to distinguish between slow crawling cells, such as fibroblasts, endothelial, and smooth muscle cells, and fast crawling cells such as *Dictyostelium* or neutrophil-like HL-60; where the typical migration velocities can differ by one to two orders of magnitude between the two types. For example, the average speed of fibroblasts is of the order of $10\mu\text{m}/\text{h}$ [8], whereas *Dictyostelium* can move at speeds on the order of $10\mu\text{m}/\text{s}$ [4]. In addition, slow crawling cells typically possess stress fibers, whereas fast crawling cells do not. This is a crucial difference to understand their mechanosensitive response.

Early experiments on fibroblasts[9] and endothelial cells[10, 11] found that these cells preferred to align their stress fibers in a direction perpendicular to the stretching. This reorientation of the stress fibers has been linked to the depolymerization and disassembly of parallel fibers[12, 13]. Nevertheless, it is also possible for the stress fibers to align parallel to the direction of stretching, as demonstrated experimentally on endothelial cells with inhibited Rho-kinase activity (which would tend to lower the myosin activity and thus the base tension)[14]. Finally, while the alignment of the stress fibers is correlated with the cell reorientation, it is by no means sufficient. This was shown by experiments on vascular smooth muscle cells, in which stress activated cation channels were inhibited, resulting in cells that were randomly oriented, even though they contained oriented stress fibers[12].

The fact that cells without stress fibers also exhibit characteristic reorientation under cyclic stretching is clear evidence that stress fiber realignment cannot be the only mechanism responsible for the reorientation. Unfortunately, the fast crawling nature of these cells makes experimental observations much more difficult, since it requires that the cell motion be tracked. Indeed it was only recently that the group of Iwadate managed to perform such experiments[4–7]. They have found that *Dictyostelium* cells prefer to migrate in the perpendicular direction. This occurs without any ordering of the dense actin-network inside the cell, but it is accompanied by the formation of dense myosin bundles at the lateral edges, preventing any pseudopod extension in those directions. Further experiments on other fast-crawling cells, such as HL-60 and Blebbistatin-treated (stress fiber less) keratocytes also found similar perpendicular alignment[6, 7]. This response has yet to be fully explained, and it is even less understood than the reorientation of slow-crawling cells, where the stress fibers seem to play a dominant role.

The mechanism responsible for the realignment is evidently cell-specific, and likely to depend on the experimental conditions. However, it is clear that it should involve several general ingredients, namely, the focal adhesion dynamics, through which the cell is able to transfer forces to and from the substrate, and the actin network and myosin induced contractility, responsible for the migration of the cell, as well as the mechanical properties of the cytoskeleton. Alternative theories have been proposed that can explain the reorientation as arising from one of these elements. For example, as a consequence of the passively stored elastic energy[15] or the forces on the focal adhesions[16, 17], with both theories capable of reproducing the same experimental data, even though they are modeling different mechanisms, under different assumptions. Furthermore, all such models seem to have been developed with slow-crawling cells in mind, where stress fibers are likely to play a crucial role, and where the motion of the cells can be decoupled from their reorientation. When considering fast crawling cells such as *Dictyostelium* or HL-60, the motility of the cell can no longer be decoupled from its reorientation. Thus, we must consider the dynamic remodeling of the relevant sub-cellular elements (e.g., the actin-cytoskeleton and the focal adhesions) under the cyclic stretching and how this affects the motion of the cell. In such cases, theoretical approaches quickly become intractable, and we must resort to computational modeling.

In this work, we extend an established phase-field model of crawling cells[18] to describe the dynamics of fast-crawling cells over substrates undergoing large amplitude cyclic deformations. We then use this model to study the reorientation dynamics as a function of frequency. Based on recent studies, which report a strong frequency dependence for the stability of focal adhesions[16, 19], we assume that the coupling to the substrate is given by a frequency-dependent detachment rate. At low frequencies, the cell and its constituent elements are able to follow the deformation and no reorientation is observed. At moderate frequencies, but below the threshold value that triggers the instability of the focal adhesions, both parallel and perpendicular orientations are stable. Increasing the frequency

over this threshold, a moderate frequency range is found over which only the perpendicular direction is stable (as seen experimentally). Furthermore, by tuning the response of the cells to detach only during fast extension, this realignment effect can be strengthened, and it is entirely reversed to favor parallel alignment if the detachment occurs during fast compression. We thus find that an asymmetry in the cellular response during loading and unloading can have a dramatic effect on their reorientation dynamics. This could be tested experimentally by employing a non-symmetric stretching protocol (i.e., fast extension accompanied by slow compression, and vice versa). Finally, upon a further increase in the frequency, only the parallel orientation is stable. The observed realignment response depends on whether the frequency of stretching is probing the shape deformation, the actin-network, or the focal adhesion dynamics. While we have used a generic model for crawling cells, and only including the response of the focal adhesion sites to the stretching, the framework we propose can be easily used with more elaborate phase-field models developed and parameterized for specific cell types. This will allow us to investigate the biomolecular and mechanical origins of the cell's mechanosensitive response in much more detail.

II. MODEL

Ever since the pioneering studies of Cahn, Hilliard, and Allen, who introduced phase-field models to study the phase-separation of binary alloys[20–23], phase-field modeling has become one of the preferred methods for physicists and material scientists to describe microstructural dynamics in systems with non-homogeneous “phases”. These phases can be used to represent any material property of interest, from a difference in density, orientational order, or chemical composition, to differences in electric or magnetic polarization, thus providing a universal framework with which to study a wide variety of phenomena. Recently, this approach has seen considerable success outside of physics, and is now actively used to address problems in biology and even medicine. Notable examples include, among others, studies on the morphodynamics of crawling cells[18, 24–27], the immune response to invading pathogens[28], axonal extension of nerve cells[29, 30], and cartilage regeneration[31], as well as tumor growth[32, 33]. In this work, we focus on the mechanosensitivity of crawling cells, and in particular on their ability to sense and respond to mechanical cues from a substrate undergoing cyclic stretching. A phase-field approach is ideally suited for this purpose, particularly for fast crawling cells, as it provides a cell-level description which can take into account the acto-myosin based propulsion mechanism, the force transmission to and from the substrate (mediated by the focal adhesion sites), as well as allowing for the large shape deformations caused by the externally applied strain. In addition, this type of modeling can easily scale upward to consider the collective dynamics of multi-cellular systems and confluent tissues[34]. In this section, we will introduce the basic phase-field model of crawling cells that we have adopted, which was originally designed to describe the motion of keratocyte-like fragments over viscoelastic substrates without any global deformation. Then, we define the periodic strain imposed on the substrate, and the extensions to the model that are required to consider crawling under such large-amplitude cyclic deformations.

A. Phase-Field Model of Cells on Viscoelastic Substrates

We adopt the 2D model originally developed by Ziebert and Aranson[26], which describes each cell using a non-conserved order parameter ρ , whose values lie between zero (outside the cell) and one (inside the cell). This allows for an implicit tracking of the boundary, avoiding many of the computational difficulties of related sharp interface methods. A free energy functional $F[\rho]$ is then associated to this order parameter and determines the driving force for its time evolution as

$$\partial_t \rho = -\Gamma \frac{\delta F[\rho]}{\delta \rho} \quad (1)$$

with Γ the mobility coefficient for ρ . This is the so-called “Model A” or time-dependent Ginzburg-Landau model[35]. To lowest order, the free energy functional takes the form

$$F[\rho] = \int [f(\rho) + D_\rho (\nabla \rho)^2] d\mathbf{x} \quad (2)$$

where $f(\rho)$ is the free energy density of the homogeneous system and the term proportional to D_ρ provides a penalty term to the formation of sharp interfaces. The free-energy density is defined to have a double-well form, representing the local stability of the two phases $\rho = 0$ and $\rho = 1$, and is given by

$$f(\rho) = \int_0^\rho (1 - \rho') (\delta[\rho] - \rho') \rho' d\rho' \quad (3)$$

where the value of δ controls the relative stability of the two. The motility of the cell is modeled by introducing an additional polar order parameter \mathbf{p} , which gives the average orientational order of the actin filament network responsible for the motion. These filaments are continuously polymerizing at the leading edge and pushing against the membrane, allowing the cell to extend forward. This requires that the cell be able to transfer the forces to the substrate, something it is able to do because the actin-network is connected to the substrate through the focal adhesion bonds. This is modeled by introducing an additional scalar field A , representing the density of adhesion bonds. Finally, the coupled set of equations for ρ , \mathbf{p} , and A are given by[18]

$$\partial_t \rho = D_\rho \nabla^2 \rho - (1 - \rho)(\delta[\rho] - \rho)\rho - \alpha(A) \nabla \rho \cdot \mathbf{p} \quad (4)$$

$$\partial_t \mathbf{p} = D_p \nabla^2 \mathbf{p} - \tau_1^{-1} \mathbf{p} - \tau_2^{-1} (1 - \rho^2) \mathbf{p} - \beta f[\nabla \rho] - \gamma (\nabla \rho \cdot \mathbf{p}) \mathbf{p} \quad (5)$$

$$\partial_t A = D_A \nabla^2 A + \rho(a_0 \|\mathbf{p}\| + a_{nl} A^2) - (d(u) + sA^2)A \quad (6)$$

where, without loss of generality we have taken $\Gamma = 1$. For the dynamics of ρ (Eq.(4)), the first two terms on the right-hand side result from taking the functional derivative of the energy functional of Eq. (2), while the last term, proportional to $\nabla \rho \cdot \mathbf{p}$, and akin to an advection term, represents the active contribution of the actin-network pushing the cell membrane. The strength with which the actin network can push on the membrane is given as a function of the local density of adhesion sites $\alpha(A) = \alpha \cdot A$. The dynamics of \mathbf{p} (Eq.(5)) is given by a simple reaction-diffusion equation, with a source term to account for the polymerization at the interface ($\propto \beta f[\nabla \rho]$), and a decay term ($\propto \tau_1^{-1}$) to account for the corresponding depolymerization. The polymerization rate is chosen to be a function of the gradient of ρ that ensures that the growth rate is bounded and limited to the interface, with

$$f[\mathbf{x}] = \frac{\mathbf{x}}{\sqrt{1 + \epsilon \|\mathbf{x}\|^2}} \quad (7)$$

As such, the maximum growth rate is given by $\simeq \beta/\sqrt{\epsilon}$. Note that an additional decay term $\propto \tau_2^{-1}(1 - \rho^2)$ is included for computational simplicity, to make sure that the actin field is non-zero only inside the cell. The last term in Eq. (5) accounts for the myosin induced bundling at the rear of the cells[26], helping to break the $\pm \mathbf{p}$ symmetry and favor polarization. A similar reaction-diffusion model is used for the concentration of adhesion sites A (Eq. (6)). Naturally, the attachment to the substrate can only occur inside of the cell: there is a linear term proportional to $a_0 \|\mathbf{p}\|^2$, since the attachments require the presence of actin, and a non-linear term $a_{nl} A^2$ to model the maturation and growth of existing bonds. For the detachment, there is a linear term that couples the dynamics of A with the substrate displacement u , and a non-linear term that saturates the total number of bonds. Finally, the δ function controlling the relative stability of the two phases is given by $\langle \cdot \rangle = \int \cdot d\mathbf{r}$

$$\delta[\rho] = \frac{1}{2} + \mu(\langle \rho \rangle - \pi r_0^2) - \sigma \|\mathbf{p}\|^2 \quad (8)$$

where the second term on the right hand side acts as a global constraint on the cell volume (with r_0 the radius of the non-polarized static cell), and the third term accounts for the myosin-induced contraction.

At first glance, the model can seem overwhelming, as it possesses over a dozen free parameters. Fortunately, a detailed analysis of this model and its variants has already been performed[36, 37], allowing us to focus on the few parameters relevant for a study on the mechanosensitivity of cells on cyclically stretched substrates. The activity of the cell can be controlled by the strength of the propulsion (α) and the rate of polymerization (β). The shape of the cell can be controlled mainly by the strength of the contractility (σ), with low (high) values resulting in fan(crescent)-like shapes. The motor-asymmetry (γ) has only a small effect on the shape or dynamics of the cell and can be considered constant without loss of generality. Of the remaining parameters appearing in the equations of motion for \mathbf{p} and A , the most important is a_0 , which sets the rate at which new adhesion sites can be formed with the substrate. For example, to consider patterned substrates, one would make this parameter be position dependent. Such a study has been presented in Ref. [18], where a viscoelastic Kelvin-Voigt model is used to describe the displacement of the substrate due to the traction forces exerted by the cell. By controlling just two parameters, the stiffness of the substrate and the rate of attachment (a_0), the authors report a wide variety of motility modes, such as steady gliding motion, stick-slip, bipedal and wandering, which have also been observed experimentally[38, 39].

B. Substrate Deformation

We consider a substrate that is being cyclically stretched along one of its axes. In most cases, this will necessarily imply a compression along the perpendicular axes, with an amplitude that depends on the Poisson's ratio ν of the

material. To describe this deformation, it is convenient to introduce Lagrangian (material) coordinates $\boldsymbol{\xi}$ to label the substrate elements. The time-dependent (Eulerian) coordinates of a given element $\boldsymbol{\xi}$ are then given by $\boldsymbol{x} = \boldsymbol{x}(\boldsymbol{\xi}, t)$, which, for the present case is given explicitly by

$$x^1 = (\xi^1 - L_x/2)(1 + \varepsilon(t)) \quad (9)$$

$$x^2 = (\xi^2 - L_y/2)(1 + \varepsilon(t))^{-\nu} \quad (10)$$

where ε is the lateral strain (along which the substrate is being actively deformed), and L_x and L_y are the (undeformed) substrate dimensions. For simplicity, we assume a sinusoidal perturbation given by

$$\varepsilon(t) = \frac{\varepsilon_0}{2}(1 - \cos(2\pi\omega t)) \quad (11)$$

We thus have two equivalent representations for our system, in terms of the body ($\boldsymbol{\xi}$) or lab (\boldsymbol{x}) frame. Given the time-dependent deformation of the substrate, it is more convenient to solve the equations of motion in the body frame, which is by definition constant, than it is to solve them in the lab frame. This is a common strategy when solving flow or elasticity problems in the presence of time-dependent boundary conditions[40–42]. However, this requires careful consideration, particularly with regards to the definition of the time derivatives.

Let \boldsymbol{e}_i and \boldsymbol{E}_I be the basis vectors in the lab and body frame, respectively, and u^i and u^I the corresponding (contravariant) components of a given vector $\boldsymbol{u} = u^i \boldsymbol{e}_i = u^I \boldsymbol{E}_I$. Throughout this work we will assume the Einstein summation convention, and reserve lower (upper) case indices for quantities in the lab (body) frame. The corresponding transformation rules are given by[43]

$$\boldsymbol{e}_i = \Lambda^I_i \boldsymbol{E}_I \quad \boldsymbol{E}_I = \Lambda^i_I \boldsymbol{e}_i \quad (12)$$

$$u^i = \Lambda^i_I u^I \quad u^I = \Lambda^I_i u^i \quad (13)$$

with $\Lambda^I_i \equiv \partial \xi^I / \partial x^i$, $\Lambda^i_I \equiv \partial x^i / \partial \xi^I$, and $\Lambda^I_i \Lambda^i_J = \delta^I_J$. The inner or scalar product between two vectors is defined as $\boldsymbol{u} \cdot \boldsymbol{v} \equiv u_I v^I = u^I v_J = G_{IJ} u^I v^J = G^{IJ} u_I v_J$, with G_{IJ} and G^{IJ} the components of the metric tensor and its inverse ($G^{IJ} G_{JK} = \delta^I_K$)

$$G_{IJ} = \Lambda^i_I \Lambda^j_J g_{ij} = \begin{pmatrix} (1 + \varepsilon(t))^2 & 0 \\ 0 & (1 + \varepsilon(t))^{-2\nu} \end{pmatrix} \quad (14)$$

where the metric tensor in the lab frame is the Euclidean metric tensor $g_{ij} = \delta_{ij}$. For what follows, we will also require the coordinate flow velocity \boldsymbol{U} , i.e., the velocity of the coordinates or the velocity of the moving substrate. In the body frame, this is defined as[41]

$$\boldsymbol{U} \equiv -\frac{\partial \boldsymbol{\xi}}{\partial t} = \begin{pmatrix} \tilde{\varepsilon}(\xi^1 - L_x/2) \\ -\nu \tilde{\varepsilon}(\xi^2 - L_y/2) \end{pmatrix} \quad (15)$$

where $\tilde{\varepsilon} = \frac{\dot{\varepsilon}}{1 + \varepsilon}$ and

$$\dot{\varepsilon}(t) = \partial_t \varepsilon(t) = 2\pi\omega \frac{\varepsilon_0}{2} \sin(2\pi\omega t) \quad (16)$$

C. Crawling Cells on Cyclically Stretched Substrates

To consider the dynamics of the cell on the cyclically stretched substrate, we begin by writing down the equations of motion in contravariant form in the body (substrate) frame of reference, replacing the time-derivatives with intrinsic time derivatives (see Appendix A), to obtain

$$\partial_t \rho = D_\rho \Delta \rho - (1 - \rho)(\delta[\rho] - \rho)\rho - \alpha(A)p^J \nabla_J \rho \quad (17)$$

$$\partial_t p^I = D_p \Delta p^I - \tau_1^{-1} p^I - \tau_2^{-1} (1 - \rho^2) p^I - \beta G^{IJ} \frac{\nabla_J \rho}{1 + \varepsilon \nabla^K \rho \nabla_K \rho} - \gamma (p^J \nabla_J \rho) p^I - p^J \nabla_J U^I \quad (18)$$

$$\partial_t A = D_A \Delta A - \tau_A^{-1} (1 - \rho^2) A + \rho (a_0 p^J p_J + a_{nl} A^2) - (d(\cdots) + s A^2) A - A \nabla_J U^J \quad (19)$$

where $\nabla_J \rho = \partial_{\xi^J} \rho = \partial_I \rho$ and $\nabla_J U^I = \partial_J U^I + \Gamma^I_{KJ} U^K$ are the components of the covariant derivative of ρ and \boldsymbol{U} , respectively (Γ^I_{JK} the connection coefficients). In addition, the Laplacian operator ∇^2 is here replaced with

the Laplace-Beltrami operator Δ . In the current case, all connection coefficients are zero ($\Gamma_{JK}^I = 0$), considerably simplifying the calculations, since $\Delta\rho = G^{JK}\partial_{\xi^J}\partial_{\xi^K}\rho$ and $\Delta p^I = G^{JK}\partial_{\xi^J}\partial_{\xi^K}p^I$. The final set of equations (17-19) are almost the same as in the original formulation (4-6), except for the last term on the right-hand side of the equations for \mathbf{p} and A , which depends on the gradient of the coordinate flow velocity ($\nabla\mathbf{U}$)

$$\nabla\mathbf{U} \equiv \begin{pmatrix} \nabla_1 U^1 & \nabla_2 U^1 \\ \nabla_1 U^2 & \nabla_2 U^2 \end{pmatrix} = \begin{pmatrix} \tilde{\varepsilon}(t) & 0 \\ 0 & -\nu\tilde{\varepsilon}(t) \end{pmatrix} \quad (20)$$

and an additional decay term (τ_A^{-1}) for the adhesion sites outside the cell. We found the latter to be necessary to avoid any spurious adhesion-mediated interactions between the cell and its periodic images, particularly when using small system sizes or low frequencies. The precise functional form for the detachment rate d will be discussed in the next subsection. The additional term in the equation for \mathbf{p} comes from the time-dependent nature of the basis vectors, whereas the term appearing in the equation for A comes from the time-dependence of the volume element, and is required to ensure the total conservation of bonds under stretching. Of note is the fact that the equations of motion are translationally invariant, i.e., there is no explicit dependence on the coordinates $\boldsymbol{\xi}$. This allows us to assume periodic boundary conditions and employ efficient pseudo-spectral methods to solve the equations. Details on the numerical implementation can be found in Appendix B.

D. Cell-Substrate Coupling

In this work, we are interested in studying the reorientation of fast-crawling cells such as *Dictyostelium*, which possess no stress fibers, on cyclically stretched substrates. Recent experiments by Iwadate et al.[7] have shown that cell reorientation occurs even though no significant orientational order is observed in the dense actin-network in the middle of the cell. Instead, the authors have reported that myosin II becomes concentrated on the stretched sides of the cell, but how this is related to the reorientation response, or which pathway the cell uses to sense the mechanical stimulation, is still not understood. However, they conclude their work by offering three possibilities for how the mechanical signals trigger the localization, (1) through the focal adhesion sites, (2) through some unidentified mechanosensitive channel, or (3) through the deformation of the actin filament network, among which they identify the latter as more likely. Here, we will consider the first option, given the obvious importance of the focal adhesions in the transmission of forces to and from the cell, and the actin-network in particular. Indeed, recent studies on slow-crawling, stress fiber containing cells, have shown that the adhesion dynamics can help to explain the experimentally observed reorientation of such cells[16, 17]. Thus, for simplicity, we will ignore any effects coming from the viscoelastic properties of the actin-network, even though it surely has a role to play in determining the reorientation response, particularly at lower frequencies[16, 19]. We therefore consider that the coupling between the cell dynamics and the substrate is due exclusively to the adhesion dynamics.

Under cyclic stretching, adhesion bonds have been shown to lose stability if the frequency is high enough[16, 19]. This is due to the high speed changes in the substrate, which prevent the formation of any stable bonds. This frequency dependence for the stability of the adhesion bonds has been linked to the strong frequency dependence of the reorientation response seen experimentally. In particular, Liu et al.[44] found that the alignment of arterial smooth muscle cells is maximized for a given value of the stretching frequency, and Jungbauer et al.[13] and Greiner et al.[45] both reported a lower threshold frequency below which no alignment is observed. Although it should be noted that the former found the response time to decrease with increasing frequency (above the lower threshold), before plateauing at an upper frequency threshold, whereas the latter found no such change.

Within the phenomenological framework we are considering, we incorporate this frequency dependent response in the form of a strain dependent detachment rate. Based on the experimental results showing a lower frequency threshold needed to observe any realignment[13, 45], and the strong frequency dependence found for the stability of focal adhesions[19], we assume that the detachment rate is sensitive only to the rate at which the substrate is being stretched. As an objective measure for this rate of stretching, we use the (Lagrangian) rate of deformation tensor \mathbf{D} , defined as the time-derivative of the Green deformation tensor (or the right Cauchy-Green tensor), which in component form is given by[46]

$$2D^I_J = G^{KI}g_{ik} \left(\Lambda_J^i \nabla_K U^k + \Lambda_K^k \nabla_J U^i \right) \quad (21)$$

In Eulerian terms, it yields the symmetric part of the velocity gradient tensor, and, as its name suggests, it provides information on the rate at which an object is being deformed or stretched. We consider that the rate of detachment d depends solely on the trace of this rate of deformation tensor $D = \text{tr}(\mathbf{D})$, i.e., how fast it is being stretched or

compressed. We assume a sharp sigmoidal response, such that $d = 0$ ($d = 1$) below (above) the critical frequency ω_c . We introduce three basic response functions

$$d^{(\pm)}(D) = \frac{d_0}{2} \left[1 + \tanh \left(b^2 (D^2 - D_c^2) \right) \right] \quad (22)$$

$$d^{(+)}(D) = \frac{d_0}{2} \left[1 + \tanh \left(b^2 (R^2(D) - D_c^2) \right) \right] \quad (23)$$

$$d^{(-)}(D) = \frac{d_0}{2} \left[1 + \tanh \left(b^2 (R^2(-D) - D_c^2) \right) \right] \quad (24)$$

with d_0 the maximum rate of detachment, D_c the critical deformation rate, $R(x) = xH(x)$ the ramp function (H the Heaviside step function), and b a numerical parameter to control the stiffness. This will allow us to distinguish the response of the cells to extension ($d^{(+)}$), compression ($d^{(-)}$), or both ($d^{(\pm)}$). In all cases, when $d = 1$, attachments to the substrate will break, which will lead to a cell that stops moving, since the propulsion term depends linearly on A , and tries to recover its circular shape.

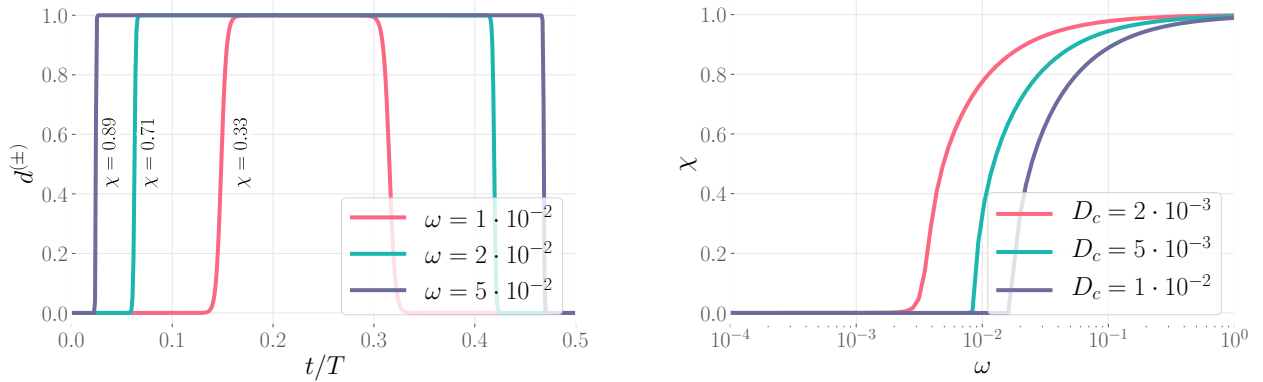


FIG. 1. (color online) (left) Detachment rate as a function of time for three different frequencies, with $D_c = 5 \cdot 10^{-3}$, $b = 10^3$, and $d = 1$. (right) Average detachment rate χ , as a function of frequency, for three different critical stretching rates D_c .

To estimate the critical frequency ω_c , we assume that the detachment functions (Eqs.(22-24)) exhibit a step-like response, which is a good approximation if b is large enough (see Figure 1). We then have $d = 1$ for $D^2 - D_c^2 \geq 0$, which leads to the following quadratic equation for $y = 1 - \cos(2\pi\omega t)$, from which we can directly compute ω_c as a function of D_c

$$B^2 = \frac{y(2-y)}{\left(1 + \frac{\varepsilon_0}{2}y\right)^2} \quad (25)$$

with $B = \frac{D_c}{\pi\omega\varepsilon_0(1-\nu)}$. The roots to this equation are given by

$$\left(1 + (B\varepsilon_0/2)^2\right) \cos(2\pi\omega t) = B^2 \frac{\varepsilon_0}{2} \left(\frac{\varepsilon_0}{2} + 1\right) \pm \sqrt{1 - B^2(1 + \varepsilon_0)} \quad (26)$$

and are real only if the term inside the square root is greater than zero, from which we can derive the critical frequency

$$\omega_c = \frac{D_c}{\varepsilon_0(1-\nu)\pi} \sqrt{1 + \varepsilon_0} \quad (27)$$

Finally, to quantify the degree to which this detachment rate affects the dynamics, we define a function χ that measures the average detachment rate over a half-cycle

$$d_0\chi = \frac{2}{T} \int_{t_0}^{t_0+T/2} d(D(t)) dt \quad (28)$$

where d is one of $d^{(\pm)}$, $d^{(+)}$, or $d^{(-)}$. Alternatively, this also provides a measure of the relative time-interval during which the cell can move. Fig. 1 shows the detachment rate as a function of time, as well as the average detachment rate as a function of frequency, Fig. 2 gives a schematic diagram of the three main quantities involved in determining the response of the cell: the time-dependent strain, the rate of deformation D , and the detachment rate $d(D)$.

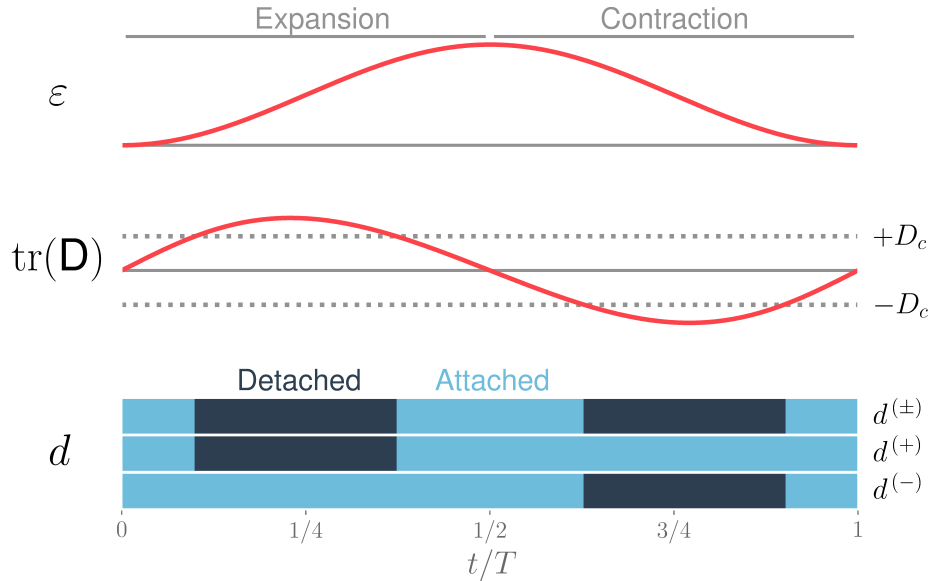


FIG. 2. (color online) Schematic representation of the adhesion/substrate coupling. From top to bottom, the stretch ratio ε , the trace of the rate-of-deformation tensor $D = \text{tr}(\mathbf{D})$, and the magnitude of the detachment rate $d(D)$, with $d = 0$ ($d = 1$) shown as light and dark blue, respectively, for three different response functions, expansion-contraction $d^{(\pm)}$, expansion $d^{(+)}$, and contraction $d^{(-)}$.

III. SIMULATION AND ANALYSIS METHOD

Parameter	Value	Description
α	4	Propulsion rate
β	$\alpha/2$	Actin nucleation rate
γ	0.5	Motors' symmetry breaking
σ	1.3	Motors' contraction
μ	0.1	Stiffness of volume conservation
D_ρ	1	Stiffness of the diffuse interface
D_p	0.2	Diffusion coefficient for \mathbf{p}
τ_1^{-1}	0.1	Degradation rate of actin
τ_2^{-1}	0.4	Decay rate of \mathbf{p} outside of cell
ϵ	37.25	Regularization of actin creation
D_A	1	Diffusion of adhesion sites
a_0	0.01	Linear adhesion attachment rate
a_{nl}	1.5	Nonlinear adhesion attachment rate
s	1	Saturation of adhesion sites
d_0	1	(Maximum) Adhesion detachment rate
τ_A^{-1}	τ_2^{-1}	Decay rate of adhesion sites outside of cell
ν	0.3	Poisson ratio
ω	0 – 0.1	Substrate Stretching frequency
ε_0	0.3	Substrate deformation amplitude
D_c	$10^{-3} - 10^{-1}$	Critical rate-of-deformation
b	10^3	Stiffness parameter for detachment rate response
r_0	15	Radius of circular initial condition

TABLE I. Default simulation parameters adapted from Ref.[18].

We consider a single cell on a cyclically stretched substrate, at various frequencies, and study the time-dependent orientation for the three different response functions introduced above $d^{(\pm)}$, $d^{(+)}$, and $d^{(-)}$. As a reference, we have also considered the case when $d = 0$, as it serves to identify to what degree the reorientation can be attributed to the passive deformation of the cell by the substrate. Since we are interested in studying the frequency dependence of the cell dynamics, we have fixed all parameters related to the cell and substrate. Unless otherwise stated, the default values are those listed in Table I, which were taken from a previous study on patterned substrates performed by Ziebert and Aranson[18]. In the absence of stretching, a polarized cell with these parameters will settle into a steady gliding motion with a fan-like shape. Regarding the stretching protocol, we follow the experiments of Iwadate et al[4], and set the Poisson's ratio at $\nu = 0.3$, with a fixed amplitude of $\varepsilon_0 = 0.3$. For all simulations we considered a single cell of circular radius $r_0 = 15$ that was initially polarized at an angle θ_0 with respect to the stretching direction ($\theta = 0$). In order to quantify the reorientation response we performed simulations for $n = 5$ different initial conditions $\theta_0 = n\pi/12$ for each set of parameter values (ω and d). The initial values for the magnitude of the polarization field and the concentration of adhesion sites were set to $p = 0.5$ and $A = 0.1$, respectively. The dimensions of the (unstretched) domain were $L_x = L_y = 100$ and we used $N = 256$ grid points along each dimension to discretize the system.

To track the orientation of the cells, we computed the center of mass as a function of time and from this, the (relative) center of mass velocity within the lab frame was obtained and used to define θ . Specifically, let $\Delta\mathbf{r}(t_0, t_1) = \mathbf{r}(t_1) - \mathbf{r}(t_0)$ be the center of mass displacement, within the lab frame, in a time interval $\Delta t = t_1 - t_0$. To compute the relative velocity of the cell \mathbf{v}_{eff} with respect to the substrate we should remove the displacement corresponding to the externally imposed strain. Consider a substrate element that at time $t = t_0$ coincides exactly with the position of the center of mass $\mathbf{r}(t_0)$. The Lagrangian coordinates for this element are $\boldsymbol{\xi}(\mathbf{r}(t_0), t_0)$. The spatial position of this element at any subsequent time t_1 is known exactly, since it follows the substrate deformation, and allows us to define the effective substrate velocity $\mathbf{u}(t_0, t_1)$ as

$$\mathbf{u}(t_0, t_1) = \frac{\mathbf{x}(\boldsymbol{\xi}(\mathbf{r}(t_0), t_0), t_1) - \mathbf{r}(t_0))}{\Delta t} \quad (29)$$

Thus, the effective velocity of the cell, within the lab frame is simply

$$\mathbf{v}_{\text{eff}}(t_0, t_1) = \frac{1}{\Delta t} [\Delta\mathbf{r}(t_0, t_1) - \Delta t \mathbf{u}(t_0, t_1)] \quad (30)$$

To obtain accurate measurements for \mathbf{v}_{eff} we made sure that the sampling time Δt was smaller than both the period of oscillation ($T = \omega^{-1}$) and the time τ required for the cell to move a distance equal to its diameter in the static case ($\omega = 0$), with v_0 the steady state velocity, such that $\tau = r_0/v_0$.

The shape deformations of the cells can be tracked by computing the aspect ratio h , defined in terms of the following shape tensor [26]

$$I^{ij} = \int (x^i - R^i)(x^j - R^j) dx dy \quad (31)$$

where $\mathbf{R} = \langle \mathbf{x}\rho(\mathbf{x}) \rangle$ is the center of mass position of the cell. The aspect ratio is then given as $h = \sqrt{\lambda_1/\lambda_2}$, where λ_1 and λ_2 are the eigenvalues of I ($\lambda_1 \geq \lambda_2$). A cell in the circular (static) state will have an aspect ratio of $h = 1$, whereas the fan-like crawling cells in the absence of stretching will present an aspect ratio closer to $h = 2$.

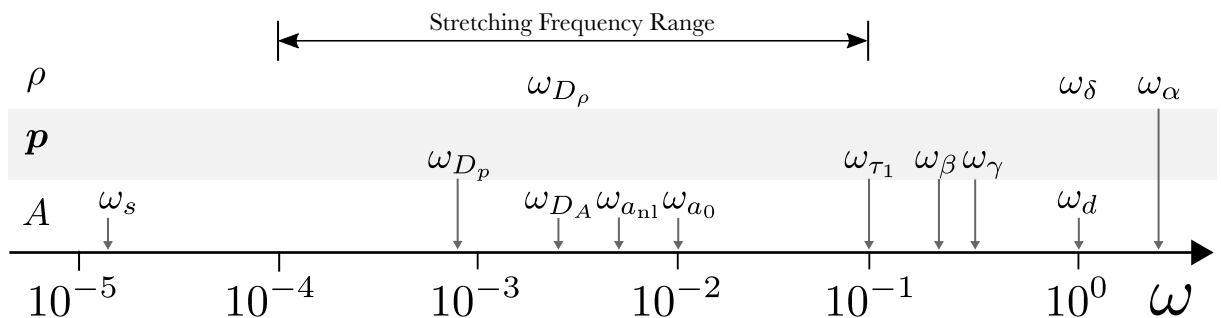


FIG. 3. Relevant time/frequency scales for the cell ρ , polarization p , and adhesion A dynamics for the default choice of parameter values given in Table I. The stretching frequency range is chosen to probe the role of the adhesion dynamics on the cell response.

To understand the reorientation dynamics, we need to consider the interplay between the dynamics of the shape deformations, the actin dynamics, and the adhesion dynamics, as well as their characteristic time-scales, and how they compare to the time-scale over which the substrate is being deformed. For this we first define the characteristic length scales in the system, the cell size $r_0 = 15$ and the interface thickness $\zeta = D_\rho^{1/2} = 1$. The characteristic time or frequency of the shape deformations is determined by the stiffness of the interface as $\omega_{D_\rho} = D_\rho r_0^{-2} \simeq 4 \cdot 10^{-3}$, as well as the time governing the retraction/expansion of the two phases $\omega_\delta = 1$. The frequency associated to the propulsion of the cell by the actin network is $\omega_\alpha = \alpha \zeta^{-3} \simeq 4$. The time-scales for the actin dynamics include the diffusion time-scale (D_p), the depolymerization rate (τ_1), the polymerization rate (β), and the asymmetry driving term (γ). They in turn yield the following characteristic frequencies, $\omega_{D_p} = D_p r_0^{-2} \simeq 9 \cdot 10^{-4}$, $\omega_{\tau_1} \simeq \tau_1^{-1} = 10^{-1}$, $\omega_\beta = \beta \epsilon^{-1/2} \simeq 3 \cdot 10^{-1}$, and $\omega_\gamma = \gamma \zeta^{-1} \simeq 5 \cdot 10^{-1}$. Finally, the frequencies associated to the adhesion dynamics are $\omega_{D_A} = D_A r_0^{-2} \simeq 4 \cdot 10^{-3}$, $\omega_{a_0} = a_0 \zeta^2 = 10^{-2}$, $\omega_{a_{nl}} = a_{nl} r_0^{-2} \simeq 7 \cdot 10^{-3}$, $\omega_s = s r_0^{-4} \simeq 2 \cdot 10^{-5}$, and $\omega_d = d = 1$. Where it should be noted that the relevant length scale for the linear attachment rate for the adhesions (a_0) is the characteristic size of the region over which the \mathbf{p} field is non-zero. Analysis of the simulations shows that this is strongly peaked near the leading edge, as the polymerization rate is proportional to $\nabla \rho$. For simplicity we have assumed that this is given by the interface width ζ , but this is just a lower bound, the real value should be slightly higher $\simeq 2 \sim 4\zeta$. In contrast, the relevant length-scale for the non-linear growth and saturation rates is the cell size r_0 . To summarize, using the default parameter values given in Table I, we can identify the following frequency regimes governing the shape (ρ), actin (\mathbf{p}), and adhesion (A) dynamics

$$\begin{aligned} \omega_{D_\rho} &\ll \omega_\delta < \omega_\alpha \\ \omega_{D_p} &\ll \omega_\gamma < \omega_{\tau_1} < \omega_\beta \\ \omega_s &\ll \omega_{D_A} < \omega_{a_{nl}} < \omega_{a_0} \ll \omega_d \end{aligned}$$

An illustration of the different characteristic frequencies is given in Fig. 3. Here, since we are interested in studying how the adhesion dynamics affect the reorientation, we will focus on stretching frequencies within the range $10^{-4} < \omega < 10^{-1}$, such that $\omega_{D_p} < \omega < \omega_{a_0}$.

IV. RESULTS

A. Passive alignment

Let us start by considering the simple case of a cell that is being passively advected by the substrate, in the absence of any direct coupling, i.e., $d = 0$. The results for this case are summarized in Fig. 4, which shows the orientation as a function of time, for various stretching frequencies ω . First, in the absence of stretching, for $\omega = 0$, the orientation of the cell is time-independent, as expected, since we have not included any source of stochasticity in the model. For non-zero frequencies, the orientation shows a clear time-variation, since it is being constantly deformed and rotated by the substrate. However, there are several distinct frequency regimes, depending on how the stretching frequency compares to the characteristic frequencies of the system, giving rise to qualitatively different realignment dynamics. At very low frequencies, $\omega \lesssim 10^{-4}$, the orientation oscillates around the initial value, but there is no stretch-induced alignment. In this case, the deformation is so slow that the cell (together with the actin network and adhesion sites) can completely follow the imposed strain. As the frequency is increased further, such that it becomes comparable to the frequency for the diffusion of orientational order ω_{D_p} , we begin to see an alignment either parallel or perpendicular to the stretching direction. In this case, the actin network is not able to rearrange fast enough to adapt to the changing shape of the cell. However, this alignment is extremely slow, with a time-scale of the order of $t/\tau \simeq 10^4$. In addition, there seems to be no preference between parallel or perpendicular directions, with the final orientation depending on the initial orientation: cells that were aligned closer to the parallel or perpendicular directions will favor those orientations. Upon increasing the frequency of oscillation to $\omega \simeq 5 \cdot 10^{-3}$, the qualitative behavior remains unchanged, but the reorientation time-scale is reduced by roughly an order of magnitude. At these frequencies, the substrate is stretching faster than the cell can relax, since $\omega > \omega_{D_p}$, so that the shape starts to become perturbed by the imposed strain. If the frequency is increased still further, we observe a clear transition, at $\omega \simeq 2 \cdot 10^{-2}$, above which all cells show a parallel alignment, regardless of the initial orientation. For such high frequencies, $\omega > \omega_{a_0} \gtrsim \omega_{a_{nl}}$, the distribution of adhesion bonds inside the cell can no longer be stabilized fast enough to keep track of the imposed deformations.

As a complement to the previous analysis, we can also consider the time-dependence of the aspect ratio h and the magnitude of the effective cell velocity v_{eff} . The time-variation of these quantities shows similar oscillations in response to the strain as does the orientation $\theta(t)$, but there is no systematic drift, with both quantities oscillating

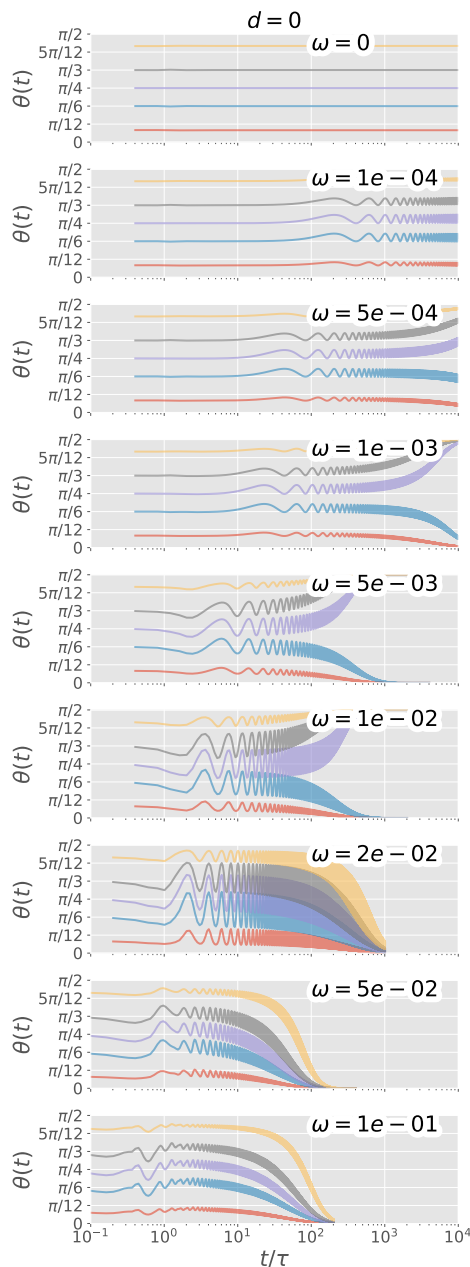


FIG. 4. (color online) Orientation θ as a function of time t for different initial polarization directions θ_0 , and various frequencies, in the absence of any specific cell-substrate coupling ($d = 0$). Default parameters given in Table I were used. Note that $\theta = 0$ ($\theta = \pi/2$) corresponds to parallel (perpendicular) alignment.

around their “equilibrium” ($\omega = 0$) values, corresponding to $h_0 \simeq 1.9$ and $v_0 \simeq 0.6$. Studying how the fluctuations in these quantities changes as a function of frequency will help us to clarify the mechanosensitive response of the cells. For this, we have plotted the maximum and minimum value of $h - 1$ and v_0 , as well as the amplitude of the corresponding oscillations, for two different initial orientations ($\theta = \pi/6$ and $\pi/3$) in Figure 5. As expected, at lower frequencies $\omega < \omega_{D_p}$ the fluctuations are negligible, as the cell is able to relax to its preferred shape faster than the substrate is being deformed. In addition, even though the cells reorient into either the parallel or perpendicular directions for $\omega \gtrsim \omega_{D_p}$, we see no difference in their shape or velocity. This means that for this frequency range the reorientation of the cell can be effectively decoupled from its translational motion. As the frequency becomes comparable to ω_{D_p} the shape of the cell begins to show oscillations, as the substrate is moving faster than it can relax. Since the velocity and motility are intimately linked, this is accompanied by a corresponding increase in the

velocity fluctuations, but this effect is much less pronounced. It is at this point where we can start to see a difference between cells oriented perpendicular or parallel to the stretching. The cell that was initially polarized at $\theta = \pi/3$ will align in the perpendicular direction and experiences considerable shape deformation but relatively small velocity fluctuations. The cell that was polarized in the $\theta = \pi/6$ direction will align in the parallel direction and shows the opposite behavior, small shape deformations but large velocity fluctuations. These tendencies increase with increasing frequency, up until $\omega \simeq \omega_{a_0}$, where the only stable orientation is the parallel one. Here, the fluctuations of the aspect ratio reach a plateau, which tells us that the cell shape is now completely unable to respond to the imposed strain. Simultaneously, at this point the stretching starts to interfere with the adhesion dynamics and this greatly amplifies the fluctuations in the velocity. We see that the cell can slow down and speed up by up to 50% with respect to their average value. This is due to the heterogeneous and unstable distribution of adhesion sites that characterize the cell at these frequencies. These fluctuations reach a maximum at $\omega \simeq 5\omega_{a_0}$, after which their amplitude shows a sharp decrease.

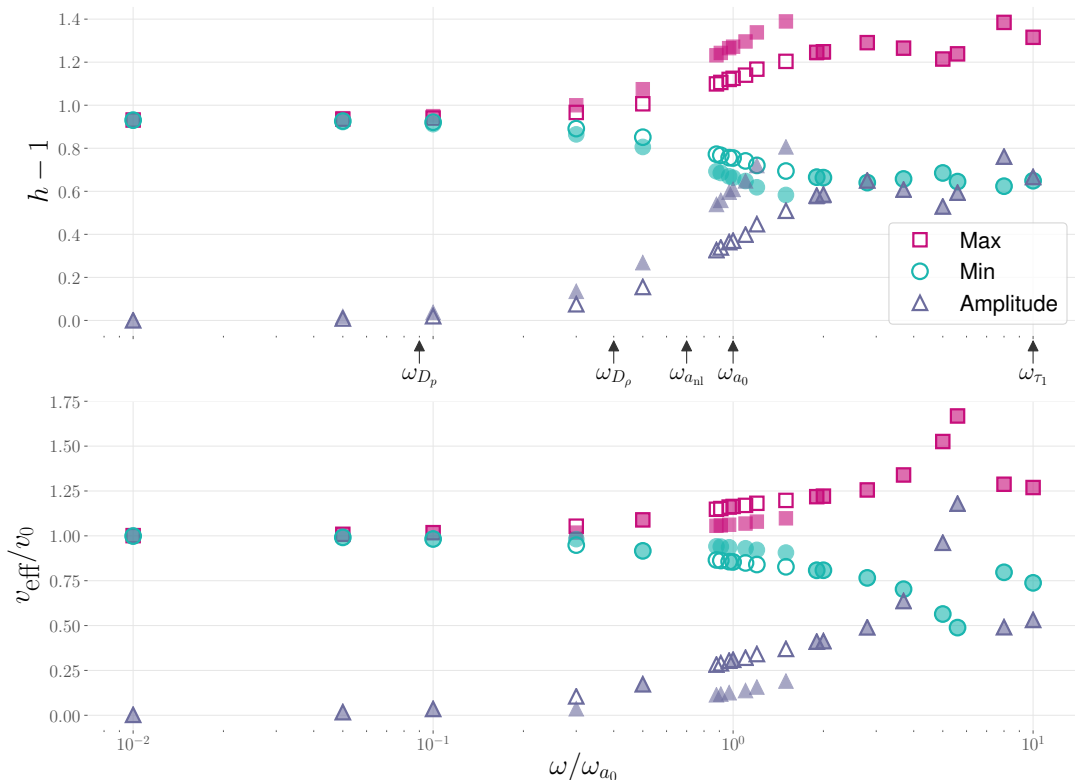


FIG. 5. (color online) Maximum, minimum, and amplitude of the (steady) oscillations of the aspect ratio h and effective velocity v_{eff} as a function of frequency ω . While there is no significant change in the average values of h or v_{eff} , the fluctuations of these quantities depend strongly on frequency. Data was obtained from the trajectories of cells initially polarized in the $\theta = \pi/6$ (open symbols) and $\theta = \pi/3$ (filled symbols) orientations, once the orientation of the cell was stabilized. The amplitude was computed as the difference between the maximum and minimum values.

The question of why the cells choose one particular orientation over another, and why the only stable orientation is the parallel one at high frequencies remains to be answered. Existing theories[15, 47–50], which focus on slow crawling cells with stress fibers, and do not consider shape deformations or the cell motility, predict that both parallel $\theta = 0$ and perpendicular $\theta = \pi/2$ orientations are solutions to the steady state equation ($d\theta/dt = 0$), together with an oblique orientation θ_f , which is a function of the system parameters. While the oblique (nearly perpendicular) orientation θ_f is usually the stable solution, under certain conditions, such as when the mechanical forces due to the substrate dominate the cellular activity, or if the substrate is very soft, the parallel orientation becomes stable[47, 48, 50]. A direct comparison with our results is not straightforward, but we also find $\theta = 0$ and $\theta = \pi/2$ as steady state solutions, with the parallel orientation the only stable one at high frequencies (at least within the frequency range we have considered). In this high frequency regime, we have seen that the cell is unable to resist the shape deformations imposed by the substrate, and that the distribution of adhesions is unstable, leading to large velocity fluctuations, even though the average velocity remains unchanged. In this limit, the forces due to the externally imposed strain

dominate any forces due to the intrinsic cell motility. Thus, our findings of a stable parallel orientation are consistent with the theoretical predictions[47, 48, 50].

In the absence of any specific cell-substrate interaction, the strong coupling that exists between shape and motility yields a preferential alignment under cyclic stretching that is strongly dependent on the relative frequency. At very low frequencies the cells and the actin network have time to readjust to the deformation, and the average migration direction is not affected. When the stretching is faster than the actin network can respond, there is a very weak reorientation process, but no preference between perpendicular or parallel directions. If the stretching is faster than the time-scale over which the cell can accommodate its shape (as defined by the stiffness of the membrane), then the reorientation is significantly faster. At even higher frequencies, where the cell cannot form and stabilize the adhesion bonds fast enough to follow the deformation, we observe that the cells align parallel to the stretching direction, regardless of initial orientation. Thus, even without any direct coupling to the substrate, there is a clear preference in the direction of migration.

B. Active alignment

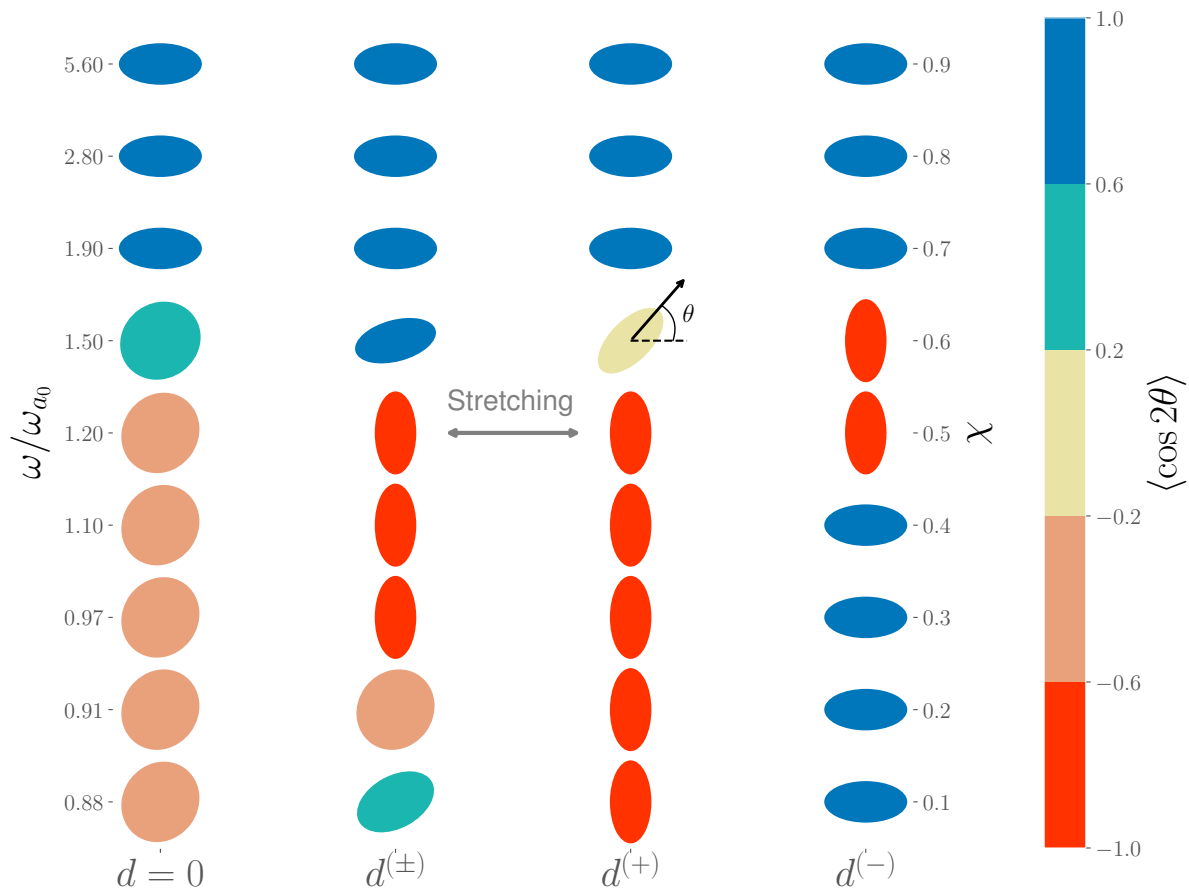


FIG. 6. (color online) Phase diagram showing the final orientation of the cells as a function of frequency ω (average detachment rate χ) and adhesion response function. Each point is specified as an ellipse, with orientation, aspect ratio, and color used to encode information on the average orientation and the spread of the orientations. Results from five simulations with distinct initial cell polarization directions ($\theta_0 = \pi/12, \pi/6, \pi/4, \pi/3, 5\pi/12$) are used for each point. The average ($\langle \theta \rangle$) and the standard deviation ($\sqrt{\langle \theta^2 \rangle}$) of the steady-state orientation is used to define the orientation of the long axis and the aspect ratio of the ellipse, respectively. In this case, small (large) standard deviations result in elongated (spherical) shapes. Finally, we also compute an orientational order parameter $\langle \cos(2\theta) \rangle$, which is 1 (-1) if all cells align parallel (perpendicular) to the stretching, and use it to color-code each ellipse. The critical stretching rate was set by $D_c = 5 \cdot 10^{-3}$, all other parameters are the same as in Fig. 4.

We now consider the reorientation of cells whose internal propulsion mechanism is actively responding to the strain

it receives from the substrate through a rate-dependent detachment rate ($d \neq 0$). This is done to model the frequency dependent stability of the focal adhesions[16, 19] As described above, Eqs.(22-24), we will consider cells that respond to either compression $d^{(-)}$ or extension $d^{(+)}$, or both $d^{(\pm)}$. By setting the threshold value $D_c(\omega_c)$ at which this response is activated, we can control the interval during which the cell is able to form attachments, and thus crawl over the substrate. Taking into account the results presented above in the absence of any direct coupling $d = 0$, for which the cells show parallel reorientation when the frequency of oscillation is greater than the frequency associated to the attachment dynamics, we can expect that a rate-dependent detachment rate will significantly affect the reorientation dynamics. We set $D_c = 5 \cdot 10^{-3}$ ($\omega_c \simeq 8 \cdot 10^{-3} \lesssim \omega_{a_0}$) and the frequency to lie in the range of $8 \cdot 10^{-3} < \omega < 6 \cdot 10^{-3}$ (χ between 0 and 1). Within this range, the only relevant time scales are those corresponding to the attachment dynamics $\omega_{a_{nl}}$ and ω_{a_0} , as the time scales for the actin and shape deformations are both slower $\omega_{D_p} < \omega_{D_r} < \omega$. For these lower frequencies, we would have $d = 0$ and the dynamics would be the same as in the passive case (Fig. 4). We have summarized the results in the phase diagram presented in Fig. 6 (see ESI 1 for the full set of trajectory data). For comparison purposes, the corresponding results for $d = 0$ have also been included. First, at high frequencies ($\omega \gtrsim 2 \cdot 10^{-2}$), we see that all cell types show parallel alignment, regardless of the specific form of the response function. In such cases, the stretching is too fast for the cell to respond ($\omega > \omega_{a_0} > \omega_p > \omega_r$), so the exact details of the attachment/detachment become irrelevant. More interesting are the results at low and intermediate frequencies. At low frequencies $8 \cdot 10^{-3} \lesssim \omega \lesssim 1.1 \cdot 10^{-2}$ ($0.1 \leq \chi \leq 0.4$), cells with $d^{(+)}$, which “resist” extension, exhibit a perpendicular alignment. In contrast, cells with $d^{(-)}$, which “resist” compression, show a parallel alignment. Within this frequency range the cyclic detachments occur over time-scales comparable to the time it takes for the cell to form and grow new attachments. It is clear that this alignment is due to the type of detachment, since cells with $d = 0$ show no preferential alignment, with $\theta = 0$ or $\theta = \pi/2$ equally likely. Furthermore, the realignment of the cells with non-zero detachment rate occurs over time-scales that are considerably shorter than those with $d = 0$.

Simulation snapshots for $\omega = 8.8 \cdot 10^{-3}$ ($\chi = 0.1$), showing the cell shape, concentration of adhesion sites, and actin orientation are given Fig. 7. Compared to cells with $d = 0$, cells showing an active response to the stretching (d^+ or d^-) exhibit more pronounced shape deformations. As can be seen from the figure, the $d^{(+)}$ cells completely detach as the substrate is extending and rotating them towards the parallel direction. However, they are able to recover their adhesions during the compression stage, when they are being rotated into the perpendicular orientation. Cells with $d^{(-)}$ show the opposite behavior. This asymmetry in the dynamics during the extension and compression stages is the cause of the reorientation. The corresponding movies are provided as Supplemental Material (ESI 2-4). For comparison purposes, movies obtained from simulations at high frequencies $\omega = 2.8 \cdot 10^{-2}$ ($\chi = 0.8$), for which all cells show parallel alignment, are also available (ESI 5-7).

For intermediate frequencies $\omega \simeq \omega_{a_0}$, with $\chi \simeq 0.5$, $d^{(+)}$ cells exhibit a transition between the low frequency response (favoring perpendicular orientations) and the high frequency response (favoring parallel orientations), resulting in a stable oblique orientation $\theta \simeq \pi/4$. Surprisingly, the $d^{(-)}$ cells also exhibit a non-monotonic behavior, even though the low and high frequency limits both show parallel orientations, at $\omega \simeq 1.2 \cdot 10^{-2}$ ($\chi \simeq 0.5$) cells align perpendicular to the stretching direction. The behavior of the $d^{(\pm)}$ cells seems more complicated, but it can roughly be understood as a competition between the opposing tendencies of $d^{(+)}$ and $d^{(-)}$ cells to orient perpendicular or parallel to the stretching at low frequencies, with the perpendicular response being dominant. This is consistent with the fact that the reorientation time-scale is much longer than that of the other cell types.

We have performed simulations for two other critical stretching rates, $D_c = 2 \cdot 10^{-3}$ ($\omega_c \simeq 3 \cdot 10^{-3}$) and $D_c = 10^{-2}$ ($\omega_c \simeq 10^{-2}$), and found similar behavior, at least in the high frequency range. However, for $\omega_c = 3 \cdot 10^{-3} \lesssim \omega_{D_p} = 4 \cdot 10^{-3}$, the stretching is now able to probe the shape-deformations. For the lowest frequency considered, $\omega = 3.4 \cdot 10^{-3}$ ($\chi = 0.1$), the $d^{(+)}$ ($d^{(-)}$) cells actually favor a parallel (perpendicular) alignment. Increasing the frequency to $\omega = 3.7 \cdot 10^{-3} \simeq \omega_{D_p}$ the system reverts back to being dominated by the adhesion dynamics, thus, if the frequency is not too high $d^{(+)}$ ($d^{(-)}$) cells will tend to align perpendicular (parallel) to the direction of stretching. We note however that for $d^{(-)}$ cells the reorientation response is less pronounced, particularly at intermediate frequencies. Again, in the high-frequency range $\omega > \omega_{a_0}$ all cells show parallel alignment.

Experimentally, the fast-crawling cells that we are modeling, such as *Dictyostelium* and HL-60[4, 5, 7], have been shown to align perpendicular to the stretching direction, just as our cells within an appropriate frequency range. In these experiments, the imposed strain was not sinusoidal in nature, but more saw-tooth like: a quick expansion of the substrate was followed by a static interval and then a slow relaxation to the original shape (such that the duty ratio was fixed to 1 : 1). Thus, there is a clear asymmetry in the rate of deformation imposed in experiments during the expansion and contraction phases. Assuming this is enough to cause a relative instability in the adhesions during expansion/contraction, it would correspond to our simulations for $d^{(+)}$. Note that the cells would not need to be able to distinguish between expansion or contraction (as we have assumed for our simulations), but only the rate of deformation, since this rate is different in the two intervals. Our simulations then provide evidence to favor the adhesion dynamics as being responsible for the reorientation. This could be tested by using a reciprocal deformation to that of the original experiments[4], with a slow expansion followed by fast contraction, for which our model ($d^{(-)}$)

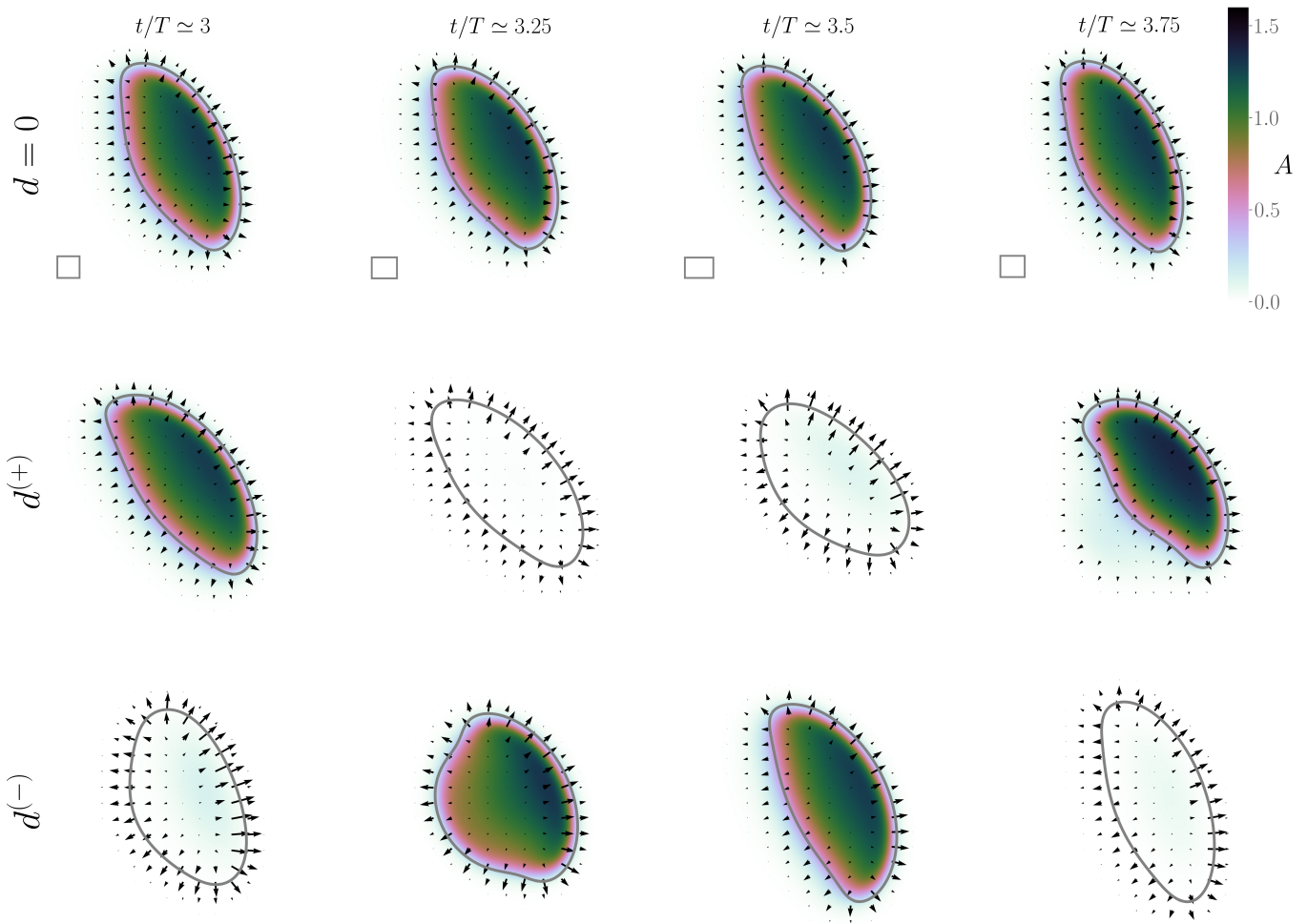


FIG. 7. Simulations snapshots for cells exhibiting passive and active responses to a periodically stretching substrate. Data was taken over one cycle between $3 \leq t/T < 4$, for cells initially polarized in the $\theta = \pi/6$ direction. From top to bottom, $d = 0$, $d^{(+)}$, and $d^{(-)}$, respectively. Solid lines show the contour of the phase-field for $\rho = 0.5$, the density map shows the concentration of adhesion sites A , and the arrows the actin orientation field \mathbf{p} . The rectangles in the top figure show the substrate deformation, scaled down by a factor of 20.

predicts a parallel orientation. Finally, while we do not claim quantitative agreement is possible with the simple model we have used here, particularly because it has not been parametrized for any specific cell type, we predict that in the limit where the adhesion dynamics dominates the response of the cells, an asymmetry in the expansion/contraction periods of the stretching can be used to selectively drive the reorientation.

V. DISCUSSION

The question of cellular realignment under a cyclically stretching substrate has attracted much attention recently due to its biological significance. Among the various possible factors or mechanisms determining this mechanosensitive response, two have been singled out: (1) the viscoelasticity of the actin filament networks and (2) the focal adhesion dynamics. This is understandable, as the former is largely responsible for the mechanical properties of the cell, and the latter provides the coupling between the cell and the substrate (through the actin-network) needed for the transfer of forces. While there has been considerable success in developing theories that can predict the reorientation dynamics of cells under cyclic stretching of the substrate, several issues remain. First, the exact mechanism responsible for the reorientation remains illusive. For example, Livne et al.[15] attribute it to the passively stored elastic energy, while Chen et al. attribute it to the forces on the focal adhesions[17, 50–52]. Both theories are able to explain the same set of experimental observations equally well, and even result in the same theoretical prediction for the orientational

dynamics, making it difficult to determine which of the two effects is the dominant one. Second, most theoretical and simulation work has so far focused on slow crawling cells which contain stress fibers, such as fibroblasts. These type of cells usually align in such a way that their stress fibers are aligned perpendicular to the stretching direction. Furthermore, since they move so slowly, their motion can be decoupled from their reorientation. Therefore, the question of how fast-crawling cells without stress fibers, such as *Dictyostelium*, reorient under cyclic stretching has remained largely unanswered. Recent experiments by Iwadate et al.[4–7] have shown that they prefer to orient perpendicular to the stretching direction. This perpendicular reorientation is observed without any corresponding alignment of the dense actin network inside of the cells.

To study how fast crawling cells respond to large amplitude cyclic deformations, we require a model that describes both the cell motion and its reorientation. For this, we need to take into account the internal machinery of the cell (e.g., the actin-network and myosin contractility), its coupling to the substrate (through the focal adhesion sites), and the accompanying shape deformations. To this end, we have established a computational framework that allows us to study the dynamics of cells using any of the phase-field models that have been recently developed recently[25, 37, 53, 54]. This phenomenological approach allows us to easily model the complex coupling between the shape and motility of the cells, as well as their interactions with the substrate. In this work, we have adopted a generic model for fast crawling cells, which is nevertheless able to reproduce a wide-variety of motility modes seen experimentally[18]. Following previous work, which found a frequency dependent instability in the focal adhesions[16, 19], and the fact that no orientational order was observed in the actin network of *Dictyostelium* under stretching, we have focused our study on the role of the adhesion dynamics on the reorientation. Given the strong frequency dependence found by Kong et al.[19], and the reports of a lower frequency threshold to observe reorientation (albeit in slow crawling cells)[13, 44], we assumed a sigmoidal response for the adhesion dynamics on the rate of deformation, such that they detach ($d \neq 0$) if the rate at which they are being deformed exceeds a given threshold. Furthermore, we can selectively tune this response so that the cells become sensitive only to compression ($d^{(-)}$) or extension ($d^{(+)}$), or both ($d^{(\pm)}$). Even using this simple coupling we are still able to obtain a non-trivial frequency dependent reorientation for our model cells. Depending on whether the cells tend to detach and stop crawling under too large extension or compression, or whether they are just being passively advected by the substrate, and how the stretching frequency compares to the characteristic frequencies associated to the shape deformation and the actin and adhesion dynamics, we can observe both perpendicular or parallel alignment, as well as oblique orientations.

As a reference, we considered first the passive case ($d = 0$). At very low frequencies, there is no reorientation, with the cell oscillating around its initial direction. As the frequency is increased, both the parallel $\theta = 0$ and perpendicular $\theta = \pi/2$ directions become steady state solutions, but there is not systematic reorientation (i.e., cells do not show any preference between either direction). This (slow) reorientation arises because the actin network can no longer follow the deformations of the substrate. At higher frequencies, past the characteristic frequency associated to the shape deformations (as given by the membrane stiffness), the reorientation time scale is considerably reduced, but there is still no preference between parallel or perpendicular directions. Finally, upon a further increase in the stretching frequency, we reach the time-scales over which the adhesion attachments are formed. It is at this point where we observe complete reorientation in the parallel direction. This parallel alignment has been predicted to occur in cases where the cellular activity is negligible compared to the forces coming from the substrate[47, 48], which is in line with our numerical predictions.

In the case of an active coupling with the substrate ($d \neq 0$), we observed complete realignment, either in the parallel or perpendicular directions, over most of the parameter range considered. Thus, our results provide further evidence for the fact that the stability of adhesion bonds can have a dramatic effect on the mechanosensitivity of crawling cells[16, 17, 19]. For all three types of responses ($d^{(\pm)}$, $d^{(+)}$, $d^{(-)}$), we were able to observe complete perpendicular alignment, as has been reported experimentally for fast-crawling cells[4, 5, 7], for low to moderate frequencies. This is particularly noticeable for the $d^{(+)}$ cells, for which the perpendicular direction is the stable orientation over a wide range of frequencies. In contrast, $d^{(-)}$ cells show a preference to align in the parallel direction. Thus, cells that resist extension (compression) will usually align perpendicular (parallel) to the direction of stretching. However, at high enough frequencies the cells always align parallel to the direction of stretching, just as the passively advected cells ($d = 0$).

Our theory predicts that in the case where the adhesion dynamics dominates the response of the cell, any asymmetry during the loading/unloading phases of the stretching can be used to align the cells along directions parallel or perpendicular to the stretching. This asymmetry can be intrinsic to the cell, if it is able to respond differently to extension and compression, or it can be due to the stretching protocol itself. This is relevant with regards to the experiments reported by Iwadate et al.[4, 5, 7], since they have not used a sinusoidal signal, with symmetric loading and unloading, but a saw-tooth like signal, with fast extension followed by a slow compression. Even if the cell cannot distinguish between extension and compression, but only the magnitude of the rate of deformation, this would correspond to our cells with the $d^{(+)}$ response. Indeed, we have shown that for moderate frequencies, these cells prefer a perpendicular orientation, as reported experimentally. This could be easily tested by repeating the experiments

with a complementary experimental protocol that had slow extension followed by fast relaxation. Such a case would correspond to our $d^{(-)}$ cells, and our theory predicts that the preferred orientation could then be switched to the parallel direction.

Our approach will prove useful to study the mechanosensitivity of fast crawling cells, since it can incorporate the salient features: (1) the elastic response of the cell, (2) the forces on the focal adhesions, (3) the active forces generated by the cell, and (4) the complex coupling between cell shape and motility. In addition, the cell-level description we propose can be trivially extended to multi-cellular systems to study the mechanosensitivity of tissues. Finally, we would like to point out that the generic model used here has not been parametrized to any particular cell type. Thus, more work is required to obtain precise quantitative comparisons with experiments. This will be the focus of future investigations, where we will consider a more detailed coupling between the cell and the substrate, as well as the effect of membrane tension and substrate elasticity, and how they affect the actin (de)polymerization rates[55].

ACKNOWLEDGMENTS

JJM would like to acknowledge fruitful discussions with Natsuhiko Yoshinaga, Koichiro Sadakane, Kenichi Yoshikawa, Matthew Turner, Takashi Taniguchi, and Simon Schnyder during the preparation of this manuscript. This work was supported by the Japan Society for the Promotion of Science (JSPS) Wakate B (17K17825) and KAKENHI (17H01083) grants, as well as the JSPS bilateral joint research projects.

Appendix A: Intrinsic Time Derivatives and Conservation Laws

To modify the equations of motion of the crawling cell for the case where the substrate itself is being stretched, we need to carefully translate the formulas to a time-dependent (non-orthonormal) coordinate system. For the spatial gradient operators, we simply replace partial derivatives (∂_{x^i}) with covariant derivatives (∇_i), however, the main issue here is how to handle the time derivatives. The material derivative should not be used, as it does not yield proper tensorial quantities. Instead, the intrinsic time-derivative should be employed[41, 56]. It defines tensorial quantities that provide the appropriate time-variation of arbitrary grade tensors along particle paths in time-dependent curvilinear coordinates. For scalars (a) and vectors (b^i), this intrinsic time-derivative takes the following form

$$\frac{\delta a}{\delta t} = \partial_t a + (u^k - U^k) \nabla_k a \quad (\text{A1})$$

$$\frac{\delta b^i}{\delta t} = \partial_t b^i + (u^k - U^k) \nabla_k b^i + b^k \nabla_k U^i \quad (\text{A2})$$

where u^k refers to the k -component of the ‘‘particle’’ velocity, U^k to that of the coordinate-flow (i.e., the coordinate-flow velocity of the moving grid), and $\nabla_k a = \partial_k a$ and $\nabla_k b^i = \partial_k b^i + \Gamma_{jk}^i b^j$ are the components of the covariant derivatives (Γ_{jk}^i the connection coefficients). In this work, given the nature of the deformation we are interested in, all connection coefficients are zero. However, as the body basis vectors are not orthonormal, since their length is changing in time, we do need to differentiate between vectors and 1-forms, or contravariant and covariant components.

Thus, we see that the advection terms are proportional to the relative velocity ($\mathbf{u} - \mathbf{U}$). In addition, if $\mathbf{U} = 0$, which corresponds to time-independent coordinates, we recover the standard material derivative $D_t \mathbf{a} = \partial_t \mathbf{a} + \mathbf{u} \cdot \nabla \mathbf{a}$. In this work, we consider the special case $\mathbf{u} = \mathbf{U}$, for which the advection term is exactly zero. This corresponds to an idealized situation of a deformable, yet inelastic substrate. That is, we impose the large-scale deformation of the substrate and ignore any deviations caused by the traction forces exerted by the cell (as these are assumed to be much smaller).

The intrinsic time-derivatives allow us to compute the change in tensorial quantities along particles paths in time-dependent curvilinear coordinates. However, when formulating conservation laws, we must consider the time-variation of extensive (integrated) material quantities. This is given by the Reynolds transport theorem. Consider the total amount of a carried by a given material element, which may be deforming in time. The total change in a is defined as[41]

$$\frac{d}{dt} \int_{V(t)} a \sqrt{g} d\xi^n = \int_{V(t)} \left(\frac{\delta a}{\delta t} + a \nabla_k u^k \right) \sqrt{g} d\xi^n \quad (\text{A3})$$

where $V(t)$ is the (time-dependent) domain of the material element under consideration, \mathbf{u} its velocity, and $g = |\det g_{ij}|$ is the determinant of the metric tensor.

Appendix B: Numerical Implementation

We outline the numerical method used to solve Eqs. (17-19). The differential equations are all of the form

$$\partial_t u = \mathcal{L}(t)u + \mathcal{G}(u, t) \quad (\text{B1})$$

where \mathcal{L} is a linear operator, which can depend on time, but is independent of u , while \mathcal{G} is the non-linear term. Applying an Euler scheme in time, treating the linear part implicitly, and the non-linear part explicitly, we have

$$\frac{u_{n+1} - u_n}{h} = \eta L_{n+1} u_{n+1} + (1 - \eta) L_n u_n + G_n \quad (\text{B2})$$

$$u_{n+1} = \left(1 - h\eta L_{n+1}\right)^{-1} \left(u_n + h[(1 - \eta)L_n u_n + G_n]\right) \quad (\text{B3})$$

where $u_n = u(t_n)$, $L_n = \mathcal{L}(t_n)$, and $G_n = \mathcal{G}(u_n, t_n)$, with h the time step and $t_n = nh$. Choosing $\eta = 0$, corresponding to an explicit calculation of the linear operator, yields

$$u_{n+1} = u_n + h[L_n u_n + G_n] \quad (\text{B4})$$

whereas $\eta = 1$, corresponding to an implicit treatment, results in

$$u_{n+1} = \left(1 - hL_{n+1}\right)^{-1} \left(u_n + hG_n\right) \quad (\text{B5})$$

We use the latter due to its improved stability. To resolve the differential operators, we employ a pseudo-spectral method[57, 58], solving the equation of motion in Fourier space, but computing all non-linear terms in real space and then transforming to Fourier space. For the equations we have considered, the linear operator is usually just the diffusion term $L \propto \Delta u$, which in Fourier space is just $\hat{L} \propto \|k\|^2 \hat{u} = G^{IJ} k_I k_J \hat{u}$ (with k the wave-vector). Fourier transforms were performed using the Fast Fourier Transform, with a typical grid size of 256×256 points on a square domain of size $L = 100$.

-
- [1] P. A. Janmey and C. A. McCulloch, Annual Review of Biomedical Engineering **9**, 1 (2007).
 - [2] S. W. Crowder, V. Leonardo, T. Whittaker, P. Papatthanasious, and M. M. Stevens, Cell Stem Cell **18**, 39 (2016).
 - [3] V. V. Hiew, S. F. B. Simat, and P. L. Teoh, Stem Cell Reviews and Reports **14**, 43 (2018).
 - [4] Y. Iwadate and S. Yumura, BioTechniques **47**, 757 (2009).
 - [5] Y. Iwadate, C. Okimura, K. Sato, Y. Nakashima, M. Tsujioka, and K. Minami, Biophysical Journal **104**, 748 (2013).
 - [6] C. Okimura and Y. Iwadate, Cell Adhesion and Migration **10**, 406 (2016).
 - [7] C. Okimura, K. Ueda, Y. Sakumura, and Y. Iwadate, Cell Adhesion and Migration **10**, 331 (2016).
 - [8] H. Ebata, A. Yamamoto, Y. Tsuji, S. Sasaki, K. Moriyama, T. Kuboki, and S. Kidoaki, Scientific Reports **8**, 5153 (2018).
 - [9] R. C. Buck, Experimental Cell Research **127**, 470 (1980).
 - [10] P. C. Dartsch and E. Betz, Basic Research in Cardiology **84**, 268 (1989).
 - [11] T. Iba and B. E. Sumpio, Microvascular Research **42**, 245 (1991).
 - [12] K. Hayakawa, N. Sato, and T. Obinata, Experimental Cell Research **268**, 104 (2001).
 - [13] S. Jungbauer, H. Gao, J. P. Spatz, and R. Kemkemer, Biophysical Journal **95**, 3470 (2008).
 - [14] C.-F. Lee, C. Haase, S. Deguchi, and R. Kaunas, Biochemical and Biophysical Research Communications **401**, 344 (2010).
 - [15] A. Livne, E. Bouchbinder, and B. Geiger, Nature Communications **5**, 3938 (2014).
 - [16] Y. Zhong, D. Kong, L. Dai, and B. Ji, Cellular and Molecular Bioengineering **4**, 442 (2011).
 - [17] B. Chen, X. Chen, and H. Gao, Nano Letters **15**, 5525 (2015).
 - [18] J. Löber, F. Ziebert, and I. S. Aranson, Soft Matter **10**, 1365 (2014).
 - [19] D. Kong, B. Ji, and L. Dai, Biophysical Journal **95**, 4034 (2008).
 - [20] J. W. Cahn and J. E. Hilliard, The Journal of Chemical Physics **28**, 258 (1958).
 - [21] J. W. Cahn, Acta Metallurgica **9**, 795 (1961).
 - [22] S. Allen and J. Cahn, Acta Metallurgica **20**, 423 (1972).
 - [23] S. M. Allen and J. W. Cahn, Scripta Metallurgica **7**, 1261 (1973).
 - [24] D. Shao, W.-J. Rappel, and H. Levine, Physical Review Letters **105**, 108104 (2010).
 - [25] D. Shao, H. Levine, and W.-J. Rappel, Proceedings of the National Academy of Sciences **109**, 6851 (2012).
 - [26] F. Ziebert, S. Swaminathan, and I. S. Aranson, Journal of The Royal Society Interface **9**, 1084 (2012).
 - [27] B. Palmieri, Y. Bresler, D. Wirtz, and M. Grant, Scientific Reports **5**, 1 (2015).
 - [28] S. Najem and M. Grant, Soft Matter **10**, 9715 (2014).
 - [29] S. Najem and M. Grant, EPL (Europhysics Letters) **102**, 16001 (2013).

- [30] T. Takaki, K. Nakagawa, Y. Morita, and E. Nakamachi, *Mechanical Engineering Journal* **2**, 15 (2015).
- [31] A. Yun, S. H. Lee, and J. Kim, *Bulletin of Mathematical Biology* **75**, 2389 (2013).
- [32] G. Sciumè, S. Shelton, W. G. Gray, C. T. Miller, F. Hussain, M. Ferrari, P. Decuzzi, and B. A. Schrefler, *New Journal of Physics* **15** (2013).
- [33] E. A. B. F. Lima, J. T. Oden, and R. C. Almeida, *Mathematical Models and Methods in Applied Sciences* **24**, 2569 (2014).
- [34] J. Löber, F. Ziebert, and I. S. Aranson, *Scientific Reports* **5**, 1 (2015).
- [35] P. M. Chaikin and T. C. Lubensky, *Principles of condensed matter physics*, 1st ed. (Cambridge University Press, New York, 1995).
- [36] I. S. Aranson, ed., *Physical Models of Cell Motility* (Springer, Cham, 2016).
- [37] F. Ziebert and I. S. Aranson, *npj Computational Materials* **2**, 1 (2016).
- [38] E. L. Barnhart, G. M. Allen, F. Jülicher, and J. A. Theriot, *Biophysical Journal* **98**, 933 (2010).
- [39] M. Riaz, M. Versaevel, D. Mohammed, K. Glinel, and S. Gabriele, *Scientific Reports* **6**, 34141 (2016).
- [40] H. Luo and T. R. Bewley, *Journal of Computational Physics* **199**, 355 (2004).
- [41] D. Venturi, *Journal of Physics A: Mathematical and Theoretical* **42** (2009).
- [42] J. J. Molina, K. Otomura, H. Shiba, H. Kobayashi, M. Sano, and R. Yamamoto, *Journal of Fluid Mechanics* **792**, 590 (2016).
- [43] B. F. Schutz, *Geometrical methods of mathematical physics*, 1st ed. (Cambridge University Press, Cambridge, 1980).
- [44] B. Liu, M.-J. Qu, K.-R. Qin, H. Li, Z.-K. Li, B.-R. Shen, and Z.-L. Jiang, *Biophysical Journal* **94**, 1497 (2008).
- [45] A. M. Greiner, H. Chen, J. P. Spatz, and R. Kemkemer, *PLoS ONE* **8**, e77328 (2013).
- [46] J. E. Marsden and T. J. R. Hughes, *Mathematical Foundations of Elasticity*, 1st ed. (Dover Publications, Inc., New York, 1994).
- [47] R. De, A. Zemel, and S. A. Safran, *Nature Physics* **3**, 655 (2007).
- [48] R. De and S. A. Safran, *Physical Review E - Statistical, Nonlinear, and Soft Matter Physics* **78**, 031923 (2008).
- [49] S. A. Safran and R. De, *Physical Review E - Statistical, Nonlinear, and Soft Matter Physics* **80**, 060901 (2009).
- [50] G.-K. Xu, B. Li, X.-Q. Feng, and H. Gao, *Biophysical journal* **111**, 1478 (2016).
- [51] J. Qian, H. Liu, Y. Lin, W. Chen, and H. Gao, *PLoS ONE* **8**, e65864 (2013).
- [52] G.-K. Xu, X.-Q. Feng, and H. Gao, *Biophysical Journal* **114**, 701 (2018).
- [53] A. Moure and H. Gomez, *Physical Review E* **94**, 042423 (2016).
- [54] S. Najem and M. Grant, *Physical Review E* **93**, 1 (2016).
- [55] B. Winkler, I. S. Aranson, and F. Ziebert, *Physica D: Nonlinear Phenomena* **318-319**, 26 (2016), arXiv:1509.00712.
- [56] R. Aris, *Vectors, Tensors, and the Basic Equations of Fluid Mechanics*, 1st ed. (Dover Publications, Inc., New York, 1989).
- [57] C. Canuto, M. Y. Hussaini, A. Quarteroni, and T. A. Zang, *Spectral Methods: Fundamentals in Single Domains*, 1st ed. (Springer, New York, 2006).
- [58] S. Bulent Biner, *Programming Phase-Field Modeling*, 1st ed. (Springer, Cham, 2017).